ISSN 0960-1317

Journal of Micromechanics and Microengineering

Structures, devices and systems

Volume 25 Number 9 September 2015

Topical review

A review of microelectromechanical systems for nanoscale mechanical characterization

Yong Zhu and Tzu-Hsuan Chang

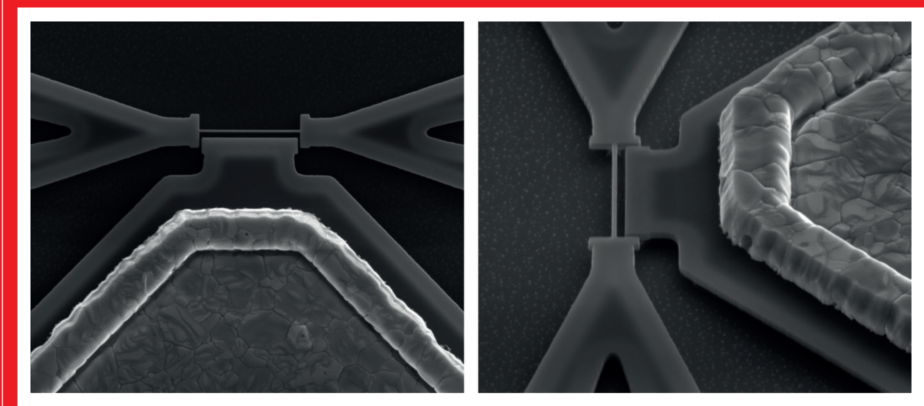

iopscience.org/jmm

IOP Publishing

IOP Publishing Journal of Micromechanics and Microengineering
J. Micromech. Microeng. **25** (2015) 095014 (12pp) doi:10.1088/0960-1317/25/9/095014

Probing contact-mode characteristics of silicon nanowire electromechanical systems with embedded piezoresistive transducers

Rui Yang[1], Tina He[1], Mary Anne Tupta[2], Carine Marcoux[3], Philippe Andreucci[3], Laurent Duraffourg[3] and Philip X-L Feng[1]

[1] Electrical Engineering, Case Western Reserve University, Cleveland, OH 44106, USA
[2] Keithley Instruments, Inc., Cleveland, OH 44139, USA
[3] CEA-Leti, Minatec Campus, 17 rue des Martyrs, 38054 Grenoble Cedex 9, France

E-mail: rui.yang@case.edu and philip.feng@case.edu

Received 7 March 2015, revised 25 May 2015
Accepted for publication 10 June 2015
Published 19 August 2015

Abstract
This article reports on a new method of monitoring nanoscale contacts in switches based on nanoelectromechanical systems, where the contact-mode switching characteristics can be recorded with the sensitive embedded piezoresistive (PZR) strain transducers. The devices are manufactured using state-of-the-art wafer-scale silicon-on-insulator technology featuring suspended silicon cantilevers and beams as switching elements and sub-100 nm thin silicon nanowires (SiNWs) as PZR transducers. Several different device configurations are studied, including mechanically 'cross'-shaped ('+'), coupled cantilever-SiNW structures, with and without local drain electrodes, and doubly clamped SiNW beams. Through detailed measurement and analysis, we demonstrate that the PZR transducers can enable detection of both mechanical and tunneling switching with multiple repeatable cycles. With the strong PZR effects in thin SiNWs, this type of device could be valuable especially for monitoring cold switching events, and when conventional direct readout of the switching events from the local gate or drain electrodes would not be efficient or sensitive, as nanoscale contacts may not be highly conductive, or may be degrading over time.

Keywords: nanoelectromechanical systems (NEMS), switch, relay, silicon nanowire (SiNW), piezoresistive (PZR) effect, transducer, nanoscale contact

(Some figures may appear in colour only in the online journal)

1. Introduction

Micro/nanoelectromechanical systems (MEMS/NEMS) offer attractive potential for ultralow-power and high-speed micro/nanoscale sensing, communication, and unconventional switching devices and logic building blocks. With the continuing miniaturization of transistors, degradation of performance and increasing power consumption have become significant issues due to the off-state leakage and large subthreshold swing, thus MEMS/NEMS switches based on mechanical contact of two surfaces are being seriously explored, as they offer zero off-state leakage and ideally abrupt switching behavior (with sharp slope and zero subthreshold swing) [1–7]. While these devices have shown mechanical switching with few, multiple, and long cycles, the contact between the two surfaces can degrade with time and the measured current could be unreliable. Therefore, having additional methods of monitoring the switching event and nanoscale contact (i.e. 'nanocontact') would provide more abundant and reliable information on the performance of the MEMS/NEMS switches.

Silicon nanowire (SiNW) NEMS have been actively explored for various applications including ultralow-power computing and resonant-mode sensing [8, 9]. Bottom-up SiNWs [10] have already been demonstrated in self-transducing

NEMS resonators because of the PZR effect in SiNWs [11], as well as in mass sensing [12]. Top-down SiNWs have also been explored, because the device can be fabricated with 8 inch wafer-scale silicon-on-insulator (SOI) technology with high yield and uniformity, facilitating very-large-scale integration (VLSI) of SiNW NEMS and co-integration with CMOS, toward a number of on-chip SiNW switching and sensing applications. SiNW NEMS resonators have shown high performance for sensing, using either the piezoresistive effect or field effect [13, 14]. SiNW also has great potential for NEMS switch applications, and we have previously demonstrated initial characterization of SiNW NEMS switches [15]. Si has been well known as a PZR material, while a very strong PZR effect has been reported more recently [16], which shows that very thin SiNWs can possess much stronger PZR effects than bulk Si. This effect has triggered much interest in exploring the origin and potential applications of the strong PZR effect in SiNWs [17–20]. Here we propose utilizing the integrated SiNW PZR transducer to monitor the nanocontact in a SiNW NEMS switch.

One main limiting factor of the lifetime of NEMS switching devices is the quality of the nanocontact [21]. Nanocontacts can be highly complicated and involve mechanical, electrical, and materials issues. Several established approaches for nanoscale materials analysis can be used for studying nanocontacts. Optical spectroscopic techniques, such as Raman spectroscopy, and other spectroscopic methods, such as x-ray photoelectron spectroscopy (XPS) and x-ray energy dispersive spectroscopy (XEDS), can be applied to perform material science analysis of the chemical composition at the contact area [22–25]. These techniques are suitable for analyzing the material properties before and after the switching events, instead of monitoring the switching event when the nanocontact is being formed and disconnected. It is also possible to monitor the surfaces or cross-sections using a scanning electron microscope (SEM) [4], transmission electron microscope (TEM) [25], or atomic force microscope (AFM) [26], which allows direct observation of the surface morphology at the nanocontact. These techniques, however, are all separate from NEMS switching operations (demanding additional measurements and instruments) and require special preparation of the samples (often damaging or totally sacrificing the switching device). Yet, these techniques could not provide information on the time-domain evolution and resolution of the switching events for a given device.

To achieve real-time, *in situ* measurement of the nanocontact, we initiate this study to explore integrated PZR transducers that may provide an extra readout (or sensing mechanism) for contact-mode NEMS switches (relays) in addition to the readout from local gate or drain electrodes. As the beams are deflected by the electrostatic force applied at the gate, they make contact to a local gate or drain, and simultaneously the strain and other effects can be read out by the naturally embedded SiNW PZR transducers. This has the following clear advantages and features. Very thin SiNWs can have a high (sometimes 'giant') PZR gauge factor (GF), remarkable strain sensitivity (approximately ppm level), wafer-scale manufacturability, and can help probe Si NEMS switches, failure modes (which have quite limited lifetime). As a result, this method could be very useful in monitoring nanocontacts, especially when the contact is mechanically unreliable due to stiction and fracture, or electrically unpredictable because of the variations in contact resistance, trapped charge in the oxide (or other insulating layer), and fusing.

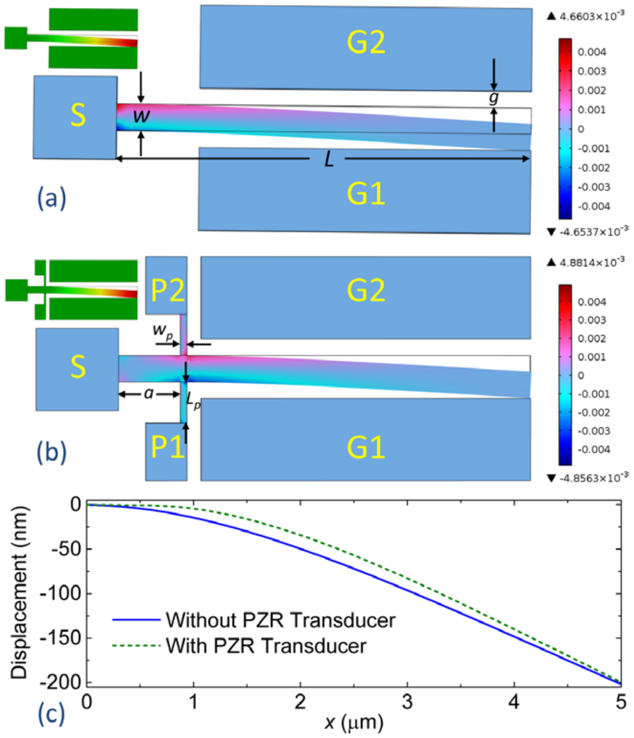

Figure 1. FEM (COMSOL) simulation of the type I two-terminal SiNW NEMS switch when the SiNW (S) is contacting gate G1. (a), (b) Strain distribution for SiNW NEMS switches (a) without PZR NW transducer and (b) with PZR NW transducers connected to the clamping ports P1 and P2. G1 and G2 are the two gates symmetrically located on both sides of the cantilever beam, and S is the source. Insets show the deflection profiles. (c) Cantilever bending profiles when the device is just switched on (S contacting G1), with and without the PZR NW transducer, respectively.

2. Basic idea and initial generic designs

2.1. Two-terminal, in-line switches: with and without NW PZR transducers

To monitor the contact in two-terminal SiNW NEMS switches, we design the PZR transducers made of SiNWs to detect the current change when the SiNW cantilever is deflected. Figure 1 shows the finite element modeling (FEM, using COMSOL) results of the strain distribution when the beam is in contact with the gate, and by comparing figure 1(a), which does not have the PZR transducer, with figure 1(b), which has it, we show that by introducing the PZR transducer, we change the strain distribution in the NEMS switch, and that when the SiNW is deflected, there is substantial strain on the PZR transducer that can cause the current change. We design

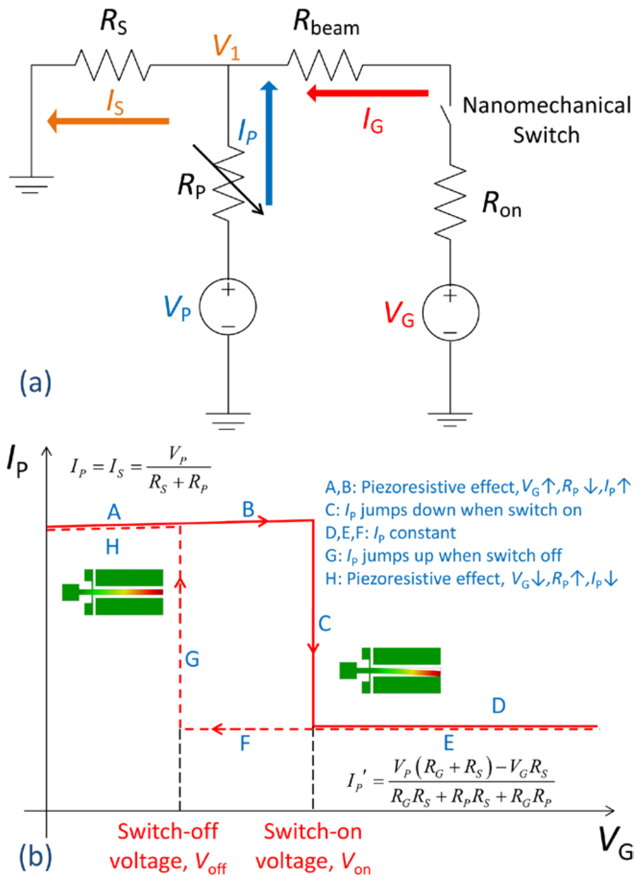

Figure 2. (a) Equivalent circuit model for type I two-terminal PZR SiNW switch measurement. (b) Expected behavior of I_P as V_G sweeps up (red solid line) and then sweeps back to 0 V (red dashed line). Insets in (b) show the deflection profiles when the switch is off (near region A) and on (near region D).

the dimensions of typical cantilever beams to have length $L = 5\,\mu$m, width $w = 320$ nm, thickness $t = 160$ nm (set by the SOI device layer thickness), and different initial air gaps, and the SiNW PZR transducer design to have length $L_p = 500$ nm, width $w_p = 80$ nm, and thickness $t_p = 160$ nm (also the same as the SOI device layer thickness). The cantilever beam is relatively wide (compared to the PZR NWs), mainly to guarantee there is enough stiffness for the cantilever to reduce the chance of stiction after contact. The width of the PZR transducer is small to minimize the effect of adding the PZR transducer on beam bending, and to make use of the strong piezoresistive effect in very thin SiNWs. The distance from the PZR transducer to the clamping point of the beam (denoted by a in figure 1(b)) is set at $a = 0.15\,L$ to maximize the stress inside the PZR transducers due to the cantilever bending [14]. Also, the PZR NW location is relatively close to the clamping point of the cantilever to minimize its effect on the cantilever deflection profile and to provide enough area for efficient gate actuation in the middle and tip area of the cantilever. The deflection profile along the cantilever length is shown in figure 1(c), demonstrating the influence of adding the PZR NW transducer on the cantilever beam's deflection profile.

Figure 2(a) is the equivalent circuit for the SiNW NEMS switches with PZR transducers shown in figure 1(b). Figure 2(b) shows the expected PZR transducer current (I_P) when we sweep the gate voltage (V_G) at G1 and measure I_P using the PZR transducer P1, which is at the same side with gate G1. When the switch is 'off' (regions A and B in figure 2(b)), the gate current is nearly zero, and I_P is described simply by:

$$I_P = I_S = \frac{V_P}{R_S + R_P}, \tag{1}$$

where V_P and R_P are respectively the PZR transducer bias voltage and the varying resistance at the SiNW PZR transducer, and I_S and R_S are respectively the current and resistance at the source electrode, which is connected to the cantilever and is grounded.

As we apply electric potential to the gate, the SiNW cantilever will be subject to an electrostatic force that bends it to the gate. The PZR transducer on the same side of the gate should be compressed, leading to a gradual decrease of R_P and increase of I_P due to the PZR effect. When the SiNW is pulled in to the gate, the switch is 'on', and the circuit can be considered as consisting of two voltage sources V_G and V_P as shown in figure 2(a), with $I_S = I_P + I_G$. The mechanical pull-in I_P and I_G of the SiNW should make both experience an abrupt change. The gate current (I_G) will increase from approximately zero to the on-state current described by

$$I_G = \frac{V_G(R_P + R_S) - V_P R_S}{R_G R_S + R_P R_S + R_G R_P}, \tag{2}$$

while the change in I_P depends on the specific voltages and resistances, and I_P after contact can be described by:

$$I_P' = \frac{V_P(R_G + R_S) - V_G R_S}{R_G R_S + R_P R_S + R_G R_P}, \tag{3}$$

where R_G is the sum of the contact resistance R_{on} and the beam resistance R_{beam}, and I_P' is the PZR transducer current when the switch is turned on.

When the switch changes from the off state to the on state, the current change in I_P can be evaluated by:

$$I_P' - I_P = \frac{R_S[-V_G(R_S + R_P) + V_P R_S]}{(R_G R_S + R_P R_S + R_G R_P)(R_P + R_S)}. \tag{4}$$

Because usually V_G is much larger than V_P, I_P' should be smaller than I_P according to equation (4), and thus the transducer current should jump down when the switch is on, as shown in region C of figure 2(b). The transducer current can even become negative if $V_P(R_G + R_S) < V_G R_S$.

After the beam makes contact with the gate, I_G usually increases from the noise floor of the instrument to the on-state current, which is usually very high because of the high V_G. Because the SiNWs are very small, it is necessary to limit the current to a maximum value to protect the SiNWs from breaking due to Joule heating. The instrument can achieve this by setting the current compliance, so that when I_G reaches the maximum current, although the programmed voltage is still sweeping up, the output current I_G does not change. Thus, the power supply is like a current source with constant I_G, and I_P will not change with programmed V_G (region D in figure 2(b)). It is the same case when the voltage is sweeping back until

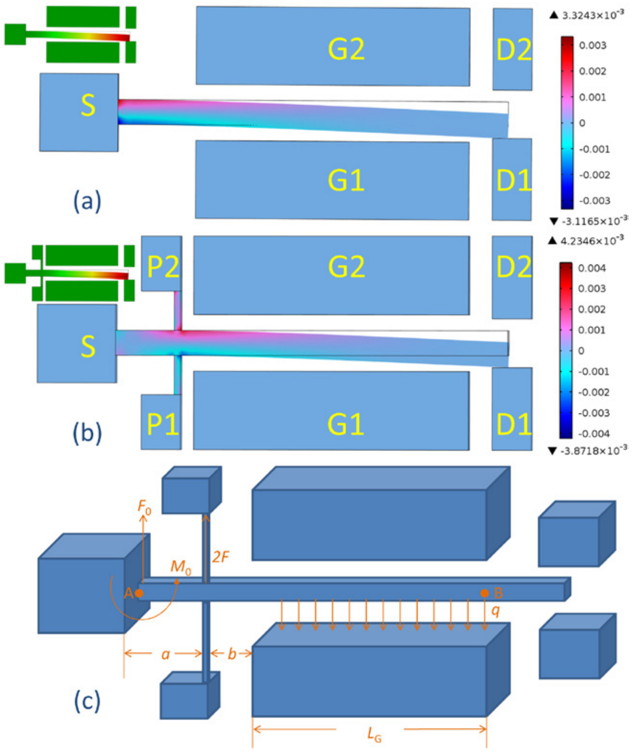

Figure 3. FEM simulation and mechanical analysis of type II three-terminal SiNW NEMS switch when G1 is used for actuation and the SiNW cantilever (S) is contacting drain D1. (a), (b) Strain distribution of SiNW switches (a) without and (b) with PZR transducers, where D1 and D2 are the two drain contacts. Insets in (a) and (b) show the deflection profiles. (c) Mechanical analysis of the system.

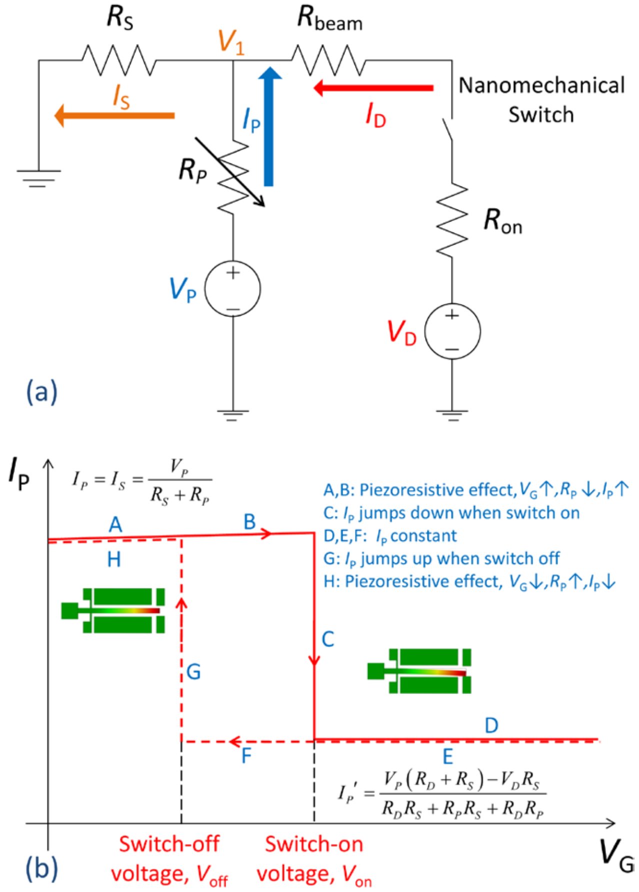

Figure 4. (a) Equivalent circuit model for the type II three-terminal SiNW switch PZR measurement, where I_D is the drain current. (b) Expected I_P with different V_G, where R_D is the sum of R_{on} and R_{beam}. Insets in (b) show the deflection profiles when the switch is off (near region A) and on (near region D).

the switch-off of voltage V_{off} (regions E and F in figure 2(b)). When the beam is released from the gate, the switch turns off, and I_P should suddenly jump up to the off-state value (region G in figure 2(b)). Here we assume that the contact resistance between the cantilever and the gate is relatively low, thus the PZR transducer current is influenced by V_G when the switch is on. If the nanocontact is not highly conductive, or is degrading a lot with time, then the strain effect on I_P should be more obvious, and I_P measured at the same side of the actuation gate should abruptly increase when the nanocontact is made due to compressive strain, and abruptly decrease when the beam is released.

2.2. Three-terminal, gate-controlled switches with and without NW PZR transducers

Besides the two-terminal switch, we have also designed three-terminal switches that should be more suitable for logic and other circuit applications, with gate as the control terminal and source to drain as the conducting channel when the switch is on. Figure 3 shows the FEM simulation results of the three-terminal switches with (figure 3(b)) and without the SiNW PZR transducer (figure 3(a)), which shows similar strain distribution to the respective two-terminal designs. The expected switching behavior should also be similar to the two-terminal devices, except that the SiNW is contacting the drain electrode when the switch is on; therefore, the drain current should show a sharp increase while the gate current should remain low and only experience minimal tunneling current (figure 4). The equivalent circuit model (figure 4(a)) and the expected PZR transducer current I_P change with sweeping V_G (figure 4(b)) explain the switching behavior of the three-terminal switch, showing similar change in I_P with two-terminal switches. Because the drain bias voltage V_D is relatively small, the current in the beam could be much smaller compared to the two-terminal switches; therefore, the current may not be higher than the compliance and the beam can be better protected from excessive heating.

The electromechanical analysis of the system is shown in figure 3(c), where the electrostatic force is considered as a uniform force between the beam and the gate using the parallel-plate capacitor assumption. By solving the equations

$$\begin{cases} \sum F_Y = 0 \Rightarrow 2F + F_0 = qL_G \\ \sum M_A = 0 \Rightarrow M_0 + 2F \cdot a = qL_G(L_G/2 + a + b) \\ \sum M_B = 0 \Rightarrow M_0 + qL_G \cdot L_G/2 \\ \quad = 2F(b + L_G) + F_0(a + b + L_G) \end{cases}, \quad (5)$$

we obtain that the force at the PZR transducer is $F = qL_G/2$ (where q is the electrostatic force per unit length),

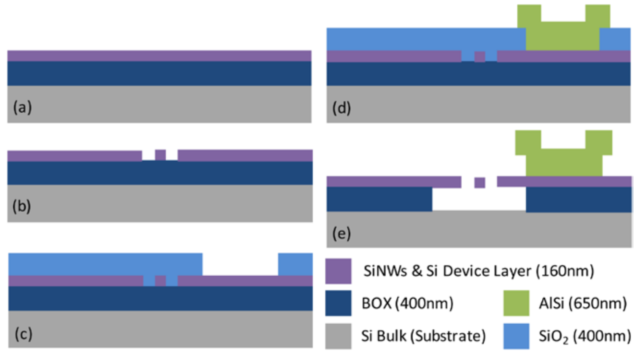

Figure 5. Simplified illustration of 8-inch wafer-scale fabrication process for enabling VLSI of suspended SiNWs: (a) SOI substrate; (b) hybrid lithography of the top Si device layer, etching Si, stripping lithography resist; (c) deposition of 400 nm SiO_2 insulation layer, lithographical pattering, etching of SiO_2 and stripping of resist; (d) deposition of 650 nm-thick AlSi, lithographical patterning, etching of AlSi, stripping of resist; and (e) etching of BOX and release of SiNWs in saturated vapor HF.

and the force at the clamp of the cantilever is zero. This confirms that the PZR transducers will be under strain when the beam deflects and will induce resistance change due to the PZR effect.

3. Fabrication process

The SiNWs are fabricated by the state-of-the-art top-down lithographic processes, with the detailed fabrication techniques illustrated in figure 5. Starting from an 8 inch SOI wafer in (1 0 0) orientation with a 160 nm Si device layer on 400 nm buried oxide (BOX), homogeneous implantation of boron (B) makes the top Si device layer a heavily doped P type at ~1×10^{19} cm^{-3}. The dopants are activated by a specific annealing step, and a resistivity of ~9 mΩ cm is achieved as compared to the undoped 10 Ω cm. The contacts are defined by deep ultraviolet (DUV) lithography, and the SiNWs are patterned by electron beam lithography (EBL), allowing a minimum feature size of 50 nm. Etching of the top Si layer is performed by anisotropic reactive ion etching (RIE). Then, another oxide layer is deposited and patterned by lithography and the AlSi is deposited to define the electrical contact. Finally, the SiNWs are released in saturated vapor hydrofluoric acid (HF) [14].

4. Measurement schemes

We have studied three types of structures, which are shown in figure 6: (a) mechanically ‘cross’ jointed/coupled two-terminal cantilever-SiNW structures; (b) ‘cross’ jointed/coupled three-terminal cantilever-SiNW structures with local drain contact and also electrostatically coupled to two gates; and (c) single-gated, doubly clamped thin SiNWs.

We carefully record the switching characteristics of the SiNW devices using a probe station connected to a high-precision semiconductor parameter analyzer (Keithley 4200 SCS) with multiple source measurement units (SMUs) (figure 6). In figures 6(a) and (c), SMU1 is connected to the gate electrode (G), providing the actuation voltage and measuring the gate current, to monitor whether the cantilever tip (of type I devices) or the SiNW midpoint (of type III devices) makes contact (or switch) to the corresponding gate. When we are performing the measurement, we sweep the gate voltage to the value we set and then sweep the voltage back to zero. With this scheme, we are able to detect the hysteresis and observe the details in the switching behavior. SMU2 is connected to the PZR transducer (P) electrode, which defines the bias voltage and records the current and strain-induced resistance change in the SiNW PZR transducer. The SiNWs that are fabricated with a similar process have been demonstrated for resonance measurement with extensive

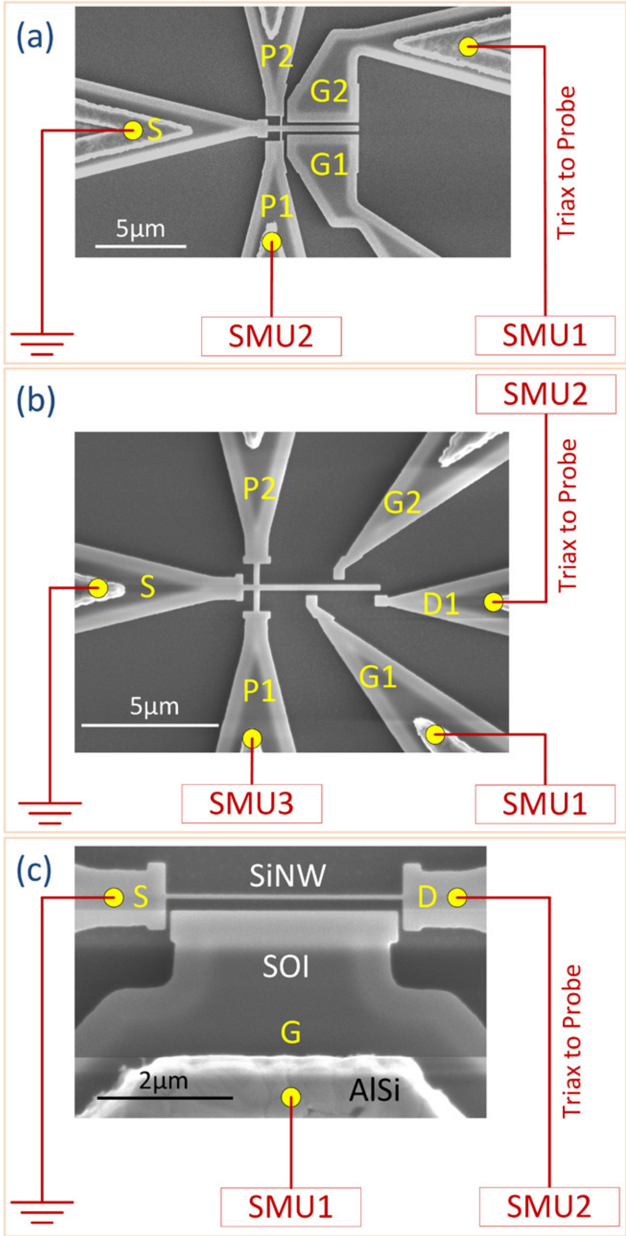

Figure 6. Illustration of the measurement schemes for (a) coupled cantilever-SiNW structures with two gates (G1 and G2) and two PZR transducers (P1 and P2), (b) coupled cantilever-SiNW structures with two gates, two PZR transducers, and a separate drain electrode (D1), and (c) doubly clamped SiNWs. Insets: SEM images of the devices.

Table 1. Dimensions and switching characteristics of measured type *I* SiNW cantilever switches, with film thickness t of 160 nm.

Device #	Width, w (nm)	Length, L (μm)	Gate length, L_G (μm)	Air gap, g (nm)	Switch-on voltage, V_{on} (V)
#1	320	5	3.9	170	29
#2	320	5	3.9	190	29; 38
#3	320	5	2.9	280	14.6; 21.4
#4 (*I-B*)	320	5	1	110	53; 9
#5 (*I-C*)	320	5	1	45	2
#6	320	5	3.9	190	74
#7 (Thin at clamp)	320	5	3.9	170	39; 67
#8 (Thin at clamp, *I-D*)	540	5	3.9	140	27
#9	320	5	1	110	19
#10 (*I-A*)	320	5	1.4	220	51; 44
#11	320	5	1.4	95	88
#12	540	5	3.9	140	17

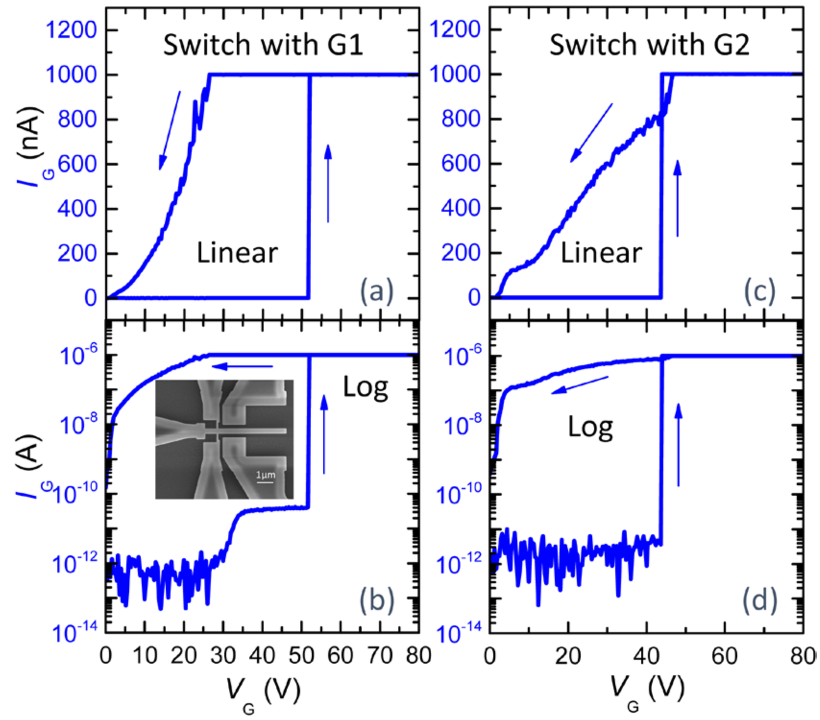

Figure 7. Switching of a type *I* cantilever-SiNW (ID: *I-A*) device with $L \approx 5\,\mu$m, $w \approx 320$ nm, and $g \approx 220$ nm actuated by V_G from both gates. (a), (b) Switching with G1 in (a) linear and (b) logarithmic scales. The beam gets stuck to G1 after the first switching. (c), (d) Switching with G2 after the first switching. The cantilever is pulled off from G1 and the device switches again by contacting G2. Inset in (b) shows the SEM image of the device.

calibration, and their material properties have been investigated [14, 19, 20]. For the SiNWs in this work with doping level of 10^{19} cm^{-3} and orientation in the <1 1 0> direction, the gauge factor is estimated to be approximately 40 to 100, and the resistivity is $\rho \approx 1.4$ mΩ cm. For the type I device in figure 6(a), SMU1 could be connected to either G1 or G2 and SMU2 could be connected to either P1 or P2 to measure the PZR current. The source (S) electrode is usually grounded. Most of the switching characteristics of our measured type I devices along with their dimensions are summarized in table 1. Figure 6(b) shows the measurement scheme of the three-terminal switch for type II devices, which is different from that of the two-terminal switches as shown in figures 6(a) and (c). The gate (G1) electrode is connected to SMU1, the local drain electrode (D1) is connected to SMU2, and the PZR transducer (P1) is connected to SMU3, which sources a bias voltage and measures the current to monitor the mechanical switching effect. All measurements are performed in ambient air at room temperature.

5. Experimental data, results, and discussions

5.1. Switching of coupled cantilever-nanowire structures

To explore type I devices (figure 6(a)), we first calibrate the 'pull-in' switching behavior by probing only the gates (G1 or G2) and the source (S) and sweeping the gate voltage, without connecting the SiNW PZR transducers.

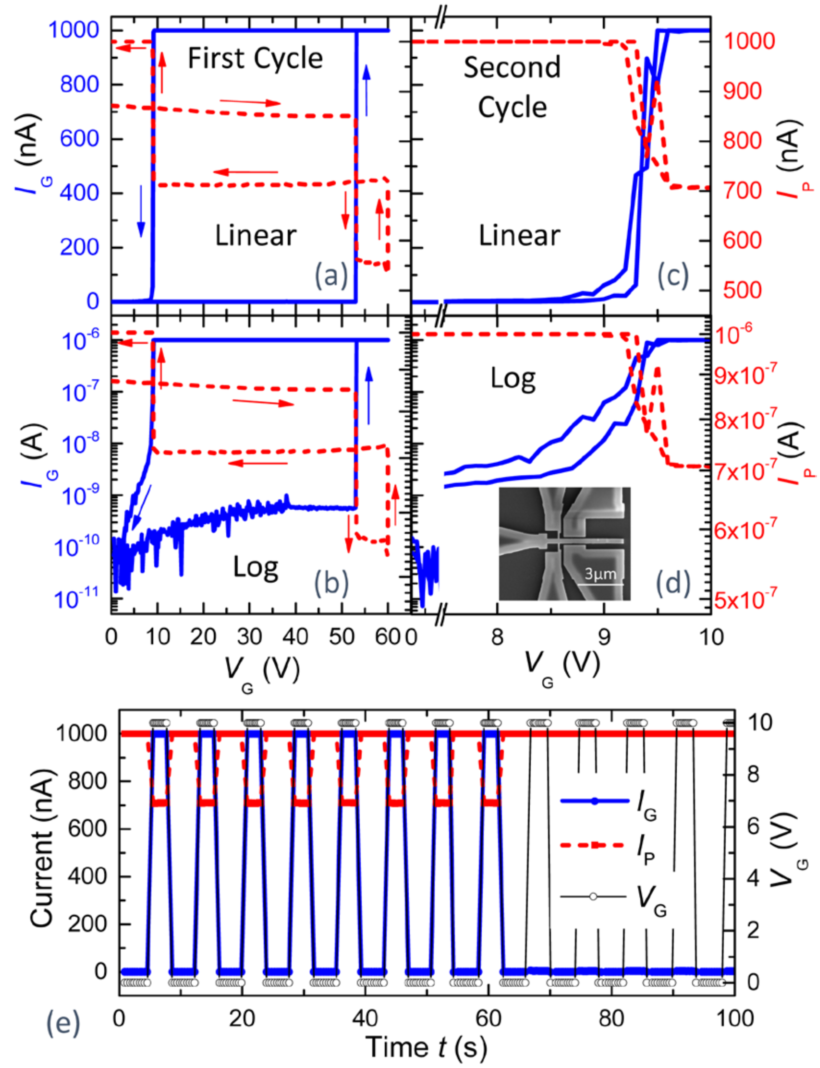

Figure 8. Measured switching characteristics of another type *I* cantilever-SiNW device (ID: *I-B*) with $L \approx 5\,\mu$m, $w \approx 320$ nm and air gap $g \approx 110$ nm. (a), (b) The first switching cycle with recorded gate current (blue solid lines) and SiNW PZR transducer current (red dashed lines) in (a) linear and (b) logarithmic scales. (c), (d) The second cycle of switching in (c) linear and (d) logarithmic scales. (e) Multi-cycle testing of the device showing switching events in the first 8 cycles, and then the gate current remains low, showing no switching characteristics. Inset in (d) shows the SEM image of the device.

For a type I device (ID: I-A) with length $L \approx 5\,\mu$m, width $w \approx 320$ nm, and air gap $g \approx 220$ nm, as we sweep the gate voltage at G1, it undergoes a two-terminal 'pull-in' switching at $V_{G1} \approx 51$ V (figure 7(a)). Then the cantilever tip gets stuck to the actuation gate G1 due to 'stiction', as shown by the I_G curve when sweeping V_G back. Because we design two complementary gates symmetrically on both sides of the cantilever, we apply actuation voltage at G2 to pull the beam off G1 and make it contact G2. Measurement results in figures 7(c) and (d) confirm that the device is successfully released from G1, and switches to G2 at $V_{G2} \approx 44$ V. This pull-off technique provides a simple and useful solution to the 'stiction' issue in contact-mode NEMS devices.

We then measure another type I cantilever device (ID: I-B) with $L \approx 5\,\mu$m, $w \approx 320$ nm, and air gap $g \approx 110$ nm using the setup as shown in figure 6(a), which not only connects the gate but also probes the PZR transducers. At the first switching cycle, we observe abrupt mechanical switching at $V_{on} \approx 53$ V, and when V_G sweeps back I_G shows clear hysteresis, with switch-off voltage $V_{off} \approx 9$ V (figures 8(a) and (b)). We get $I_{on}/I_{off} \approx 10^4$, which is limited by the noise floor and the maximum current set to protect the device from excessive Joule heating. The PZR transducer current I_P measured at P1 also shows the switching event. First, it slowly decreases as we sweep up V_G from 0 V to 53 V, corresponding to a total increase in resistance of 2.4%. The gauge factor of the SiNWs can be expressed as

$$\mathrm{GF} = (1 + \nu) + \frac{1}{\varepsilon}\frac{\Delta\rho}{\rho}, \qquad (6)$$

where ν is the Poisson ratio (0.26 for SiNW), ε is the strain, and ρ is the resistivity. For semiconductors like SiNWs, the second term is dominant. Thus, for our device with GF of ~40–100, when the cantilever deflects, the SiNW PZR transducer connected to the clamping port P1 is under compressive strain, so the resistivity should decrease and I_{P1} should increase. Yet the measured I_{P1} result with V_G swept in the range of 0 to 53 V shows increasing resistance and decreasing I_{P1}, different from

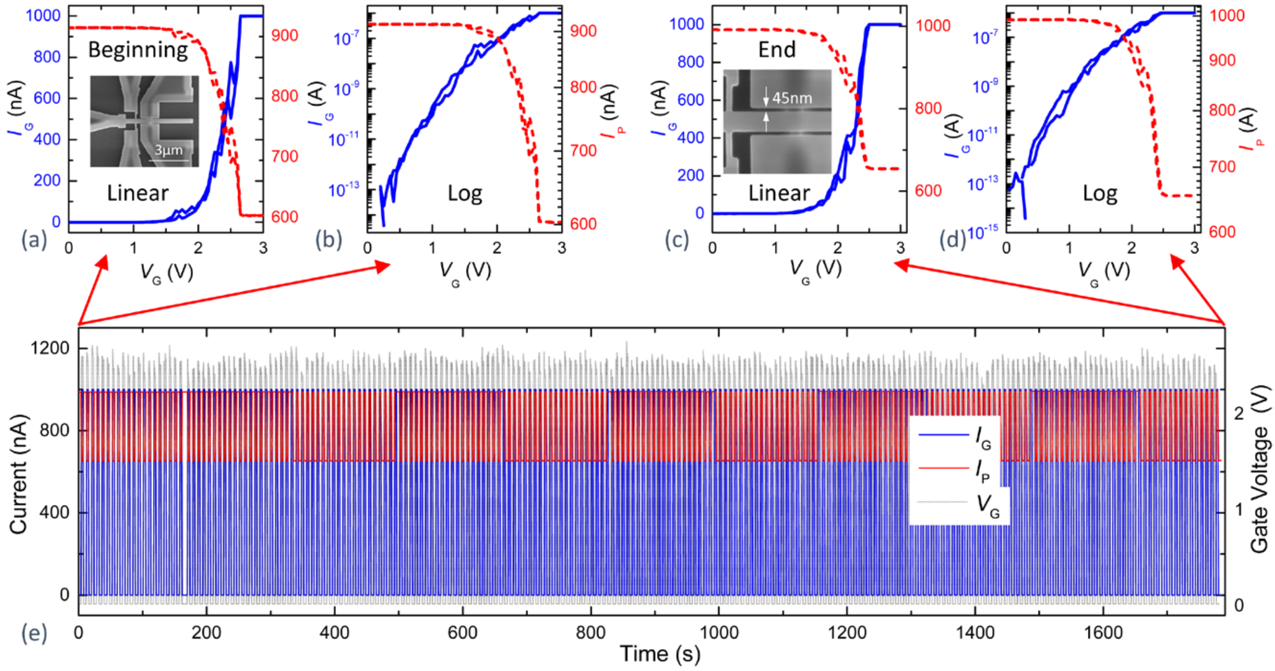

Figure 9. Measured switching characteristics of another type *I* mechanically coupled cantilever-SiNW device (ID: *I-C*) with $L \approx 5\,\mu$m, $w \approx 320$ nm, and air gap $g \approx 45$ nm, showing measurement of multiple switching cycles. (a), (b) The switching cycle before the long cycle measurement with recorded gate current (blue solid lines) and PZR SiNW current (red dashed lines) in (a) linear and (b) logarithmic scales. (c), (d) The switching cycle after the long cycle measurement in (c) linear and (d) logarithmic scales. (e) Multi-cycle periodic measurement of the device (similar to figure 8(e)) with recorded switching of more than 240 cycles. Insets in (a) and (c) are the SEM images of the device, showing the narrow air gap.

what the model in figure 2 predicts according to GF, which could be attributed to other side effects. One possible explanation is that because the air gap between the PZR SiNW and the gate electrode is not very large (~300 nm), the positive gate voltage could have an electric field effect on the SiNW and the SiNW may be partially depleted, which will increase the resistance of the SiNW and decrease the current. This effect can be avoided by designing the PZR transducer further away from the gates G1 and G2, or even on the other side of the actuating gate.

As we continue to sweep V_G to $V_{on} \approx 53$ V, I_G increases to the current compliance set by the instrument (1 μA), and I_P jumps down abruptly, which is consistent with the predicted I_P in figure 2. Then, as V_G sweeps back after contact, I_P shows an abrupt increase at $V_{off} \approx 9$ V when the beam releases (confirmed with I_G curve), which is also consistent with our model. We find that as we start to sweep the gate voltage back from $V_G \approx 60$ V, I_P shows an abrupt increase from ~540 nA to ~720 nA. To explain this effect, we carefully examine the whole switching behavior and also note that when we sweep V_G from 9 V back to 0 V, I_P is at a higher level (beyond the current compliance of 1 μA) than the I_P value attained when we sweep up V_G from 0 V to 9 V. Also, in the second cycle of switching in figures 8(c) and (d), the starting I_P is higher than the current compliance. This may suggest certain changes in the SiNW, which could come from a few possible origins. First, current-induced electrothermal annealing of the SiNW may cause the resistance to decrease, since the SiNWs are very thin and the current density is high (~7800 A cm^{-2} for 1 μA current in the PZR NW transducer). Second, because the measurement is performed in air, there could be an adsorption or desorption process that could couple to the electrothermal properties of the SiNW and affect its resistance. As we switch the device again, we find that the V_{on} value in the second cycle of switching (figures 8(c) and (d)) is similar to the V_{off} value in the first switching cycle, and there is very small hysteresis. The second cycle of switching is less abrupt, shown by the increasing tunneling current in I_G in the subthreshold region, which is likely caused by the change in the shape of the cantilever. Still, $I_{on}/I_{off} \approx 10^4$ is achieved, similar to the first cycle. I_P also changes as the device is switching, which decreases when the switch is on. The I_P at $V_G < V_{on}$ is higher than the current limit, so we cannot observe any change. A square-wave of V_G is then applied for quasi-static periodic switching (figure 8(e)), where V_G varies from 0 V (switch is off) to 10 V (switch is on) periodically, with a period of ~8 s. This device has switched for 8 cycles in the periodic switching measurement, which is evident in both I_G and I_P current, and then shows no switching event for V_G up to 10 V. The results show that the switching events and nanocontacts can be monitored with both I_G and I_P.

Figure 9 shows the measured data from yet another type *I* device (*I-C*) with $L \approx 5\,\mu$m, $w \approx 320$ nm, and air gap $g \approx 45$ nm. The device has a low switch-on voltage of $V_{on} \approx 2$ V, with V_{off} almost the same as V_{on} (figures 9(a)–(d)). The relatively low voltage is probably due to the small air gap, and we also find that this switching behavior is not as abrupt as that shown in figures 7 and 8. Both the SEM images of the specific device (figures 9(a) and (c), insets) and the I_G curves in linear and logarithmic scales suggest that the very narrow coupling air

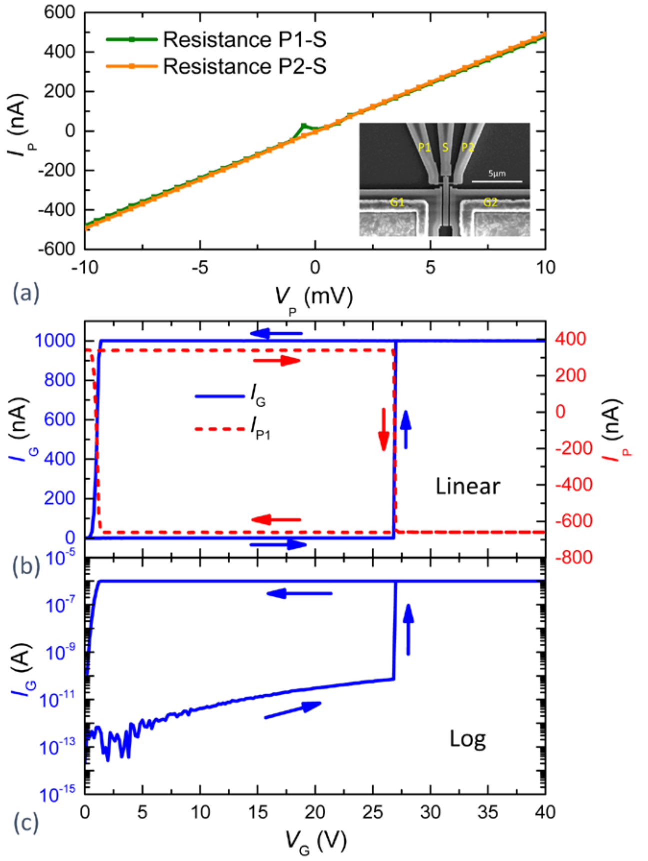

Figure 10. (a) Measured resistances from P1 and P2 to S of another type *I* device (ID: *I-D*). Inset: SEM image of the device. (b), (c) Measured switching characteristics of the device in (b) linear and (c) logarithmic scales.

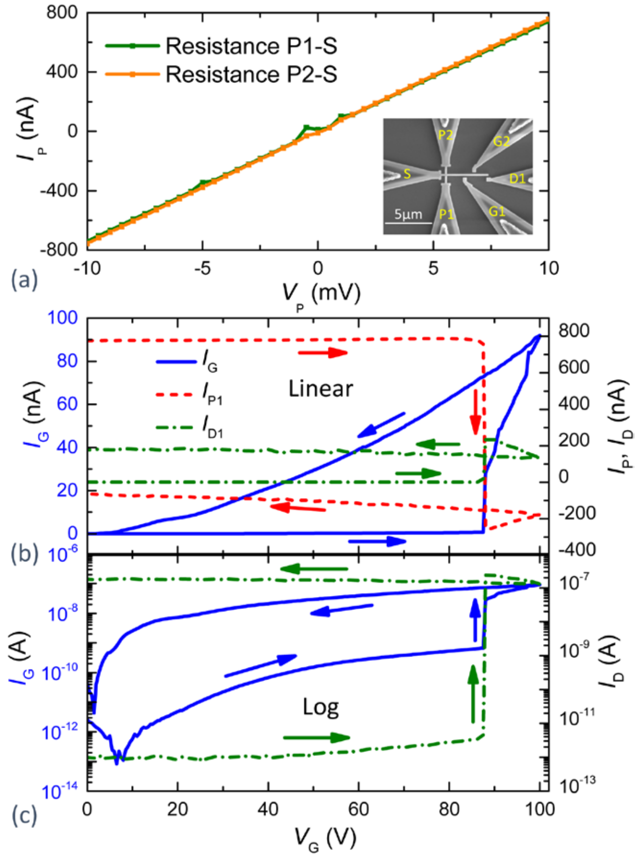

Figure 11. Switching behavior of a type II device (three-terminal cantilever-nanowire structure) with independent gates and drains. (a) Measured resistances from the PZR transducers P1 and P2 to S. Inset: SEM image of the device. (b), (c) Measured switching characteristics with currents measured with PZR transducer at P1 (red dashed lines) and drain current recorded at the local drain contact D1 (olive dash dot lines) in (b) linear and (c) logarithmic scales.

gap of the device might have created a channel for tunneling-like switching. We note from the SEM image in figure 9(c) inset that process-related residues in this very narrow air gap might have facilitated tunneling to occur. Although the data strongly suggest a tunneling effect, the mechanical movement could also happen at the same time, which forms a unique type of switching possibly combining tunneling and mechanical switching, and presents a very high I_{on}/I_{off} ratio of >10^6. When the switch is on, I_G increases and I_P decreases as expected. The periodic switching data using a similar method of measurement as in figure 8(e) are shown in figure 9(e), proving that this type of switching is highly repeatable. This device has switched for multiple cycles with such quasi-static measurements, with at least >240 cycles recorded, without observable degradation in switching behavior (device is still alive).

Another measured type *I* device (*I-D*) is shown in the figure 10(a) inset. The device has $L \approx 5\,\mu$m, $w \approx 540$ nm, and $g \approx 140$ nm, and the SiNW cantilever local stiffness is lowered by narrowing the clamping part. This type of structure will potentially reduce V_{on} of the device. We first measure the resistances of the two PZR transducers by probing/wiring (figure 10(a)) only the PZR transducers (P1 or P2) and the source (S), and sweeping V_P. The results show that the resistances of the two PZR transducers are almost the same (~20 kΩ), confirming the uniformity of our fabrication process. We then measure the switching behavior as demonstrated in figures 10(b) and (c). The device shows an abrupt increase in I_G and decrease in I_{P1} at $V_{on} \approx 27$ V, and I_P even becomes negative, which, according to the previous analysis, is likely due to the high V_G or small contact resistance.

5.2. Switching of coupled cantilever-nanowire structures with independent gate and drain

The type II, three-terminal switch device shown in the figure 11(a) inset has cantilever $L \approx 5\,\mu$m, $w \approx 200$ nm, PZR transducer length $L_P \approx 0.78\,\mu$m, width $w_P \approx 200$ nm, air gap between gate and cantilever $g_{GS} \approx 180$ nm, and air gap between drain and cantilever $g_{DS} \approx 180$ nm, and is measured using the setup shown in figure 6(b). Before the three-terminal switch measurement, we first perform resistance measurement on the two PZR transducers (figure 11(a)), which also shows that the resistances of the two PZR transducers are quite similar (~13 kΩ).

As we sweep the gate voltage, the PZR transducer shows an approximately 1.4% increase in I_P as the cantilever is bending. For this device, the gate electrode is relatively far away from the PZR transducer with ~1.7 μm air gap, so there

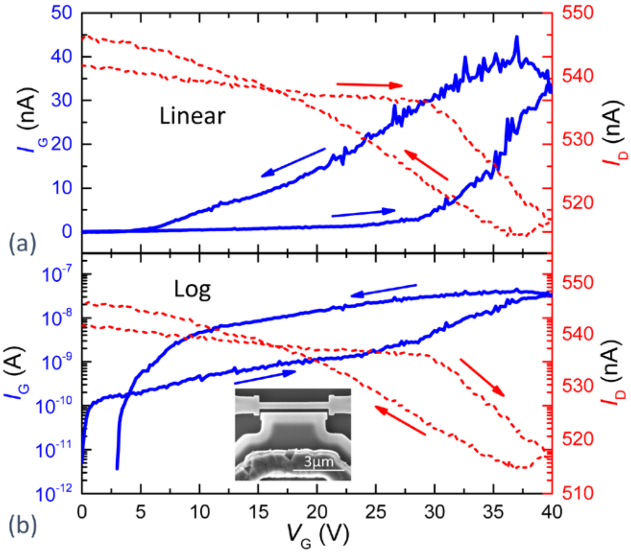

Figure 12. Two-terminal switching in a type III doubly clamped SiNW with $L \approx 3.5\,\mu$m, $w = 320$ nm, and $g \approx 200$ nm in (a) linear and (b) logarithmic scales. Inset in (b) shows the SEM image of the device.

will be very small gating effect, which proves our assumption for figure 8(a), on explaining the decrease of I_P when sweeping up V_G. When the switch is on, the SiNW beam is supposed to only contact the drain (D1) electrode while the data in figures 11(b) and (c) show that the beam is contacting both G1 and D1. This could possibly be improved by engineering the beam stiffness, changing the position of the gate electrode, and making the air gap between the gate and the beam slightly larger than that between the drain and the beam. The switching event can be shown by I_G, I_D, and I_P at the same time, with I_D suddenly increasing and I_P decreasing. V_{on} is high (~88 V), probably because the gate area is small, and therefore not efficient enough in producing the electrostatic force to deform the beam. This can be improved by increasing the length of the gate electrode.

5.3. Pull-in switching of doubly clamped Si nanowires

We have also measured type III doubly clamped SiNWs, as shown in figure 12, using the configuration in figure 6(c). Since the beams are doubly clamped, they usually have high stiffness and therefore a relatively high 'pull-in' voltage. Figure 12 shows measured results of a doubly clamped SiNW switch with $L \approx 3.5\,\mu$m, $w = 320$ nm, and $g \approx 200$ nm. The device shows $V_{on} \approx 30$ V, which is not quite high voltage, but the switching is not very abrupt, which probably indicates that when the beam is deflected toward the gate to make contact, the contact region may be very small for this beam (which is wide and stiff); there is tunneling current through the native oxide in the contact region. The red arrow in figure 12 indicates how I_D changes as V_G sweeps, which shows that I_D decreases and I_G increases. The switching behavior of an SiNW device that is 80 nm wide, thinner, and doubly clamped has been measured and described [15], and shows abrupt switching behavior. This type of switching

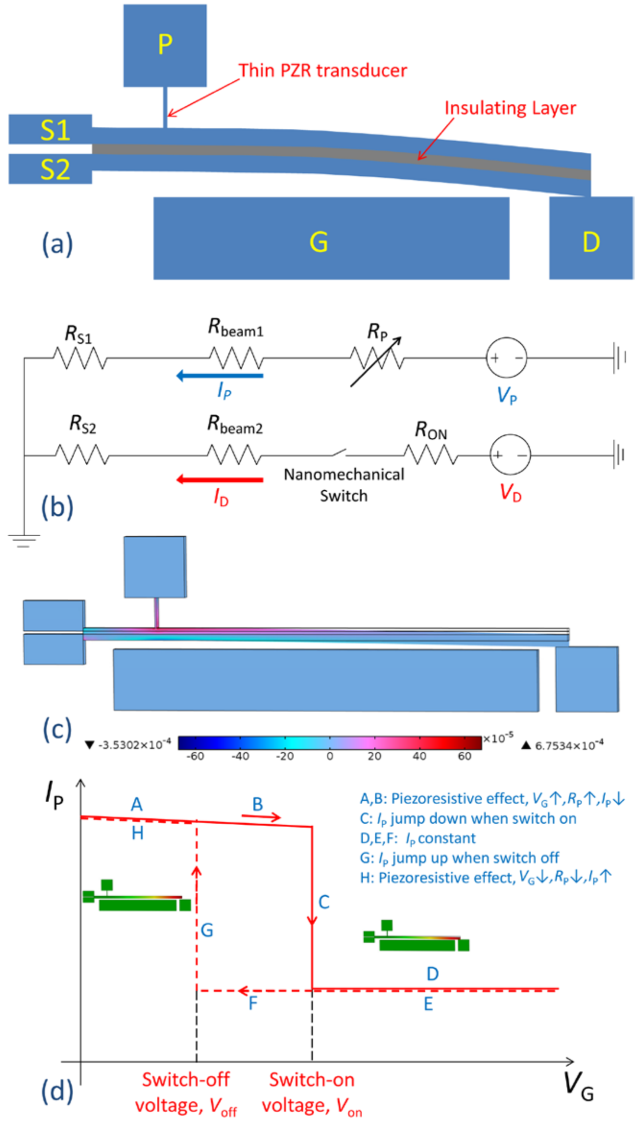

Figure 13. Future design of the three-terminal switch with PZR transducers for better performance. (a) Illustration of the design using composite beams with an insulating layer sandwiched between two conductive layers. (b) Equivalent circuit model of the design in (a), showing that I_P is only dependent on R_P. (c) COMSOL simulation of the strain distribution in the structure described in (a). (d) Expected I_P with sweeping V_G. Insets in (d) show deflection profiles when the switch is off (near region A) and on (near region D).

device will require more optimization and further analysis to boost the functionality and performance compared to the cantilever devices. For example, increasing the beam length to larger than $10\,\mu$m and shrinking the width of the beam and the air gap to ~50 nm (which has been prototyped, albeit not at the wafer-scale manufacturing [4]) can achieve operations at low switch-on voltage. We also note that other doubly clamped SiNW NEMS switches [27] were recently reported with two-mode operations: mechanical pull-in switching and electric field-induced depletion-based switching. All these initial explorations are interesting and encouraging; further engineering efforts will continue to enable low-voltage and multi-cycle NEMS switching.

6. Design and discussion on future devices

Based on our measurements, we design future devices that are expected to exhibit better performance in monitoring the contact in SiNW NEMS switches with the integrated PZR transducers. The measured data shown previously demonstrate that the PZR transducer currents used for monitoring contact are complicated by the gate (two-terminal switch) or the drain (three-terminal switch) voltages when the switch is on. To decouple the PZR transducer from the gate or drain voltage, we propose the composite beam structure (figure 13(a)), where the beam contains an insulating layer between two conducting layers. As shown in figure 13(b), I_P is only dependent on the change in piezoresistor's resistance R_P if we keep V_P constant; therefore, a more clear PZR effect should be observed when the beam is bending. This purpose can also be achieved by heavily doping the two outside layers while keeping the middle layer undoped or lightly doped, which avoids using another insulating material. Also, the design is able to introduce enough strain at a reasonable voltage (figure 13(c)). The expected I_P–V_G characteristic for this design is demonstrated in figure 13(d), showing that I_P purely comes from the PZR effect, and it captures the whole switching event, with abrupt decrease when nanocontact is formed due to tensile strain and abrupt increase when the beam is released.

7. Conclusions

We have designed and measured both cross-shaped ('+') mechanically coupled cantilever-SiNW structures with and without local drain contacts and doubly clamped SiNW beams as contact-mode NEMS switches with integrated SiNW PZR transducers as a new additional readout for monitoring the nanocontact behavior during switching operations. The sensitive integrated SiNW PZR transducer provides an efficient readout of the strain induced in it when the cantilever beam is deflected and the NEMS switching event is occurring. Analysis and FEM simulations are used to model the switching behavior of these devices. The integrated SiNW PZR transducers offer a new means for monitoring nanocontacts in contact-mode NEMS devices in real time, and have the potential to be further engineered to attain multifunctionalities and high performance.

Acknowledgment

We are grateful for the support of DARPA (NEMS Program, Grant No. D11AP00292), NSF (Grant No. CCF-1116102), DTRA Basic Scientific Research Program (Grant No. HDTRA1-15-1-0039), Case School of Engineering, a CSC Fellowship (No. 2011625071), and the French Research Agency (Carnot-NEMS Research Program).

References

[1] King Liu T-J *et al* 2010 Prospects for MEM logic switch technology *IEEE Int. Electron Devices Meeting (IEDM 2010) (6–8 December 2010)* pp 424–7

[2] Lin Y, Li W, Ren Z and Nguyen C T-C 2008 A resonance dynamical approach to faster, more reliable micromechanical switches *IEEE Int. Frequency Control Symp. (IFCS 2008) (19–21 May 2008)* pp 640–5

[3] Lee T-H, Bhunia S and Mehregany M 2010 Electromechanical computing at 500 °C with SiC *Science* **329** 1316–8

[4] Feng X L, Matheny M H, Zorman C A, Mehregany M and Roukes M L 2010 Low voltage nanoelectromechanical switches based on silicon carbide nanowires *Nano Lett.* **10** 2891–6

[5] He T *et al* 2013 Silicon carbide (SiC) nanoelectromechanical switches and logic gates with long cycles and robust performance in ambient air and at high temperature *IEEE Int. Electron Devices Meeting (IEDM 2013) (9–11 December 2013)* paper 4.6 p 108–11

[6] He T *et al* 2013 Time-domain AC characterization of silicon carbide (SiC) nanoelectromechanical switches toward high speed operations *17th Int. Conf. on Solid-State Sensors, Actuators and Microsystems (Transducers 2013) (16–20 June 2013)* pp 669–72

[7] He T *et al* 2013 Robust silicon carbide (SiC) nanoelectromechanical switches with long cycles in ambient and high temperature conditions *26th IEEE Int. Conf. on Micro Electro Mechanical Systems (MEMS 2013) (20–24 January 2013)* pp 516–9

[8] Ernst T *et al* 2008 Novel Si-based nanowire devices: will they serve ultimate MOSFETs scaling or ultimate hybrid integration *IEEE Int. Electron Devices Meeting (IEDM 2008) (15–17 December 2008)* pp 745–8

[9] Arcamone J *et al* 2011 VLSI silicon multi-gas analyzer coupling gas chromatography and NEMS detectors *IEEE Int. Electron Devices Meeting (IEDM) (5–7 December 2011)* paper 29.3 p 669–72

[10] Paulo A S *et al* 2007 Suspended mechanical structures based on elastic silicon nanowire arrays *Nano Lett.* **7** 1100–4

[11] He R, Feng X L, Roukes M L and Yang P 2008 Self-transducing silicon nanowire electromechanical systems at room temperature *Nano Lett.* **8** 1756–61

[12] Feng X L, He R, Yang P and Roukes M L 2007 Very high frequency silicon nanowire electromechanical resonators *Nano Lett.* **7** 1953–59

[13] Colinet E *et al* 2009 Ultra-sensitive capacitive detection based on SGMOSFET compatible with front-end CMOS process *IEEE J. Solid-State Circuits* **44** 247–57

[14] Mile E *et al* 2010 In-plane nanoelectromechanical resonators based on silicon nanowire piezoresistive detection *Nanotechnology* **21** 165504

[15] Yang R *et al* 2013 Silicon nanowire electromechanical switches with integrated piezoresistive transducers *26th IEEE Int. Conf. on Micro Electro Mechanical Systems (MEMS 2013) (20–24 January 2013)* pp 229–32

[16] He R and Yang P 2006 Giant piezoresistance effect in silicon nanowires *Nat. Nanotechnol.* **1** 42–6

[17] Milne J S, Rowe A C H, Arscott S and Renner C H 2010 Giant piezoresistance effects in silicon nanowires and microwires *Phys. Rev. Lett.* **105** 226802

[18] Neuzil P, Wong C C and Reboud J 2010 Electrically controlled giant piezoresistance in silicon nanowires *Nano Lett.* **10** 1248–52

[19] Koumela A *et al* 2011 Piezoresistance of top-down suspended Si nanowires *Nanotechnology* **22** 395701

[20] Koumela A *et al* 2013 High frequency top-down junction-less silicon nanowire resonators *Nanotechnology* **24** 435203

[21] Jang W W *et al* 2008 Fabrication and characterization of a nanoelectromechanical switch with 15 nm thick suspension air gap *Appl. Phys. Lett.* **92** 103110

[22] Stockle R M, Suh Y D, Deckert V and Zenobi R 2000 Nanoscale chemical analysis by tip-enhanced Raman spectroscopy *Chem. Phys. Lett.* **318** 131–6

[23] Lee N *et al* 2007 High contrast scanning nano-Raman spectroscopy of silicon *J. Raman Spectrosc.* **38** 789–96

[24] Tang C Y, Kwon Y N and Leckie J O 2007 Probing the nano-and micro-scales of reverse osmosis membranes-a comprehensive characterization of physiochemical properties of uncoated and coated membranes by XPS, TEM, ATR-FTIR, and streaming potential measurements *J. Membrane Sci.* **287** 146–56

[25] Ho G W, Wong A S, Wee A T and Welland M E 2004 Self-assembled growth of coaxial crystalline nanowires *Nano Lett.* **4** 2023–6

[26] Bhushan B, Kasai T, Kulik G, Barbieri L and Hoffmann P 2005 AFM study of perfluoroalkylsilane and alkylsilane self-assembled monolayers for anti-stiction in MEMS/NEMS *Ultramicroscopy* **105** 176–88

[27] Boodhoo L *et al* 2015 Fabrication and characterisation of suspended narrow silicon nanowire channels for low-power nano-electro-mechanical (NEM) switch applications *Microelectron. Eng.* **145** 66–70